Icarus 294 (2017) 201–208

Contents lists available at ScienceDirect

Icarus

journal homepage: www.elsevier.com/locate/icarus

CO_2 ice structure and density under Martian atmospheric conditions

T.P. Mangan[a,*], C.G. Salzmann[b], J.M.C. Plane[a], B.J. Murray[c]

[a] School of Chemistry, University of Leeds, LS2 9JT, UK
[b] Department of Chemistry. University College London, WC1H 0AJ, UK
[c] School of Earth and Environment, University of Leeds, LS2 9JT, UK

ARTICLE INFO

Article history:
Received 21 October 2016
Revised 8 March 2017
Accepted 10 March 2017
Available online 11 March 2017

Keywords:
Mars
Mars atmosphere
Mars climate
Ices
Atmospheres
Composition

ABSTRACT

Clouds composed of CO_2 ice form throughout the Martian atmosphere. In the mesosphere, CO_2 ice clouds are thought to form via heterogeneous ice nucleation on nanoparticles of meteoric origin at temperatures often below 100 K. Lower altitude CO_2 ice clouds in the wintertime polar regions form up to around 145 K and lead to the build-up of the polar ice caps. However, the crystal structure and related fundamental properties of CO_2 ice under Martian conditions are poorly characterised. Here we present X-ray diffraction (XRD) measurements of CO_2 ice, grown via deposition from the vapour phase under temperature and pressure conditions analogous to the Martian mesosphere. A crystalline cubic structure was determined, consistent with the low-pressure polymorph (CO_2-I, space group *Pa*-3 (No. 205)). CO_2 deposited at temperatures of 80-130 K and pressures of 0.01–1 mbar was consistent with dry ice and previous literature measurements, thus removing the possibility of a more complicated phase diagram for CO_2 in this region. At 80 K, a lattice parameter of 5.578 ± 0.002 Å, cell volume of 173.554 ± 0.19 Å^3 and density of 1.684 ± 0.002 g cm^{-3} was determined. Using these measurements, we determined the thermal expansion of CO_2 across 80–130 K that allowed for a fit of CO_2 ice density measurements across a larger temperature range (80–195 K) when combined with literature data (CO_2 density = $1.72391 - 2.53 \times 10^{-4} T - 2.87 \times 10^{-6} T^2$). Temperature-dependent CO_2 density values are used to estimate sedimentation velocities and heterogeneous ice nucleation rates, showing an increase in nucleation rate of up to a factor of 1000 when compared to commonly used literature values. This temperature-dependent equation of state is therefore suggested for use in future studies of Martian mesospheric CO_2 clouds. Finally, we discuss the possible shapes of crystals of CO_2 ice in the Martian atmosphere and show that a range of shapes including cubes and octahedra as well as a combination of the two in the form of cubo-octahedra are likely.

1. Introduction

Visible and Infra-red measurements have been used to unambiguously identify the presence of clouds composed of CO_2 ice in the Martian Atmosphere (Herr and Pimentel, 1970; Montmessin et al., 2007). CO_2 ice clouds can impact the radiative budget of Mars and are inherently linked to the atmospheric circulation of the planet (Forget and Pierrehumbert, 1997; Spiga et al., 2012). Microphysically, Martian CO_2 clouds are quite distinct from water clouds which form on Mars and other planets, since CO_2 is the major atmospheric constituent and therefore crystal growth is not diffusion limited. In addition, CO_2 ice formation and precipitation impacts the pressure of the entire Martian atmosphere, with changes of approximately 20% over the seasons (Tillman et al., 1993). Mars is the only place in our solar system where CO_2 clouds have been observed, but CO_2 ice is thought to be present in icy satellites in the outer solar system (Johnson, 1996; McCord et al., 1998) and the interstellar medium (Chiar, 1997), as well as making up the polar ice caps on Mars which can be up to 10 m thick at the south pole (Byrne and Ingersoll, 2003; Leighton and Murray, 1966).

Three distinct types of mesospheric CO_2 ice clouds are known to exist, the main two types occurring during the day around the equator (65–85 km altitude with mean CO_2 ice particle radii ≤ 3 µm) and in sub-tropical regions at night (80-100 km altitude with mean CO_2 ice particle radii of approximately 100 nm) (Clancy et al., 2007; Montmessin et al., 2006; Montmessin et al., 2007; Sefton-Nash et al., 2013; Vincendon et al., 2011). The third, less frequently observed, type occurs in mid-latitude regions at altitudes of 53–62 km with mean particle radii of 2 µm (Maattanen et al., 2010; McConnochie et al., 2010). Mesospheric CO_2 ice clouds

* Corresponding author.
E-mail addresses: ee09tm@leeds.ac.uk (T.P. Mangan), b.j.murray@leeds.ac.uk (B.J. Murray).

http://dx.doi.org/10.1016/j.icarus.2017.03.012

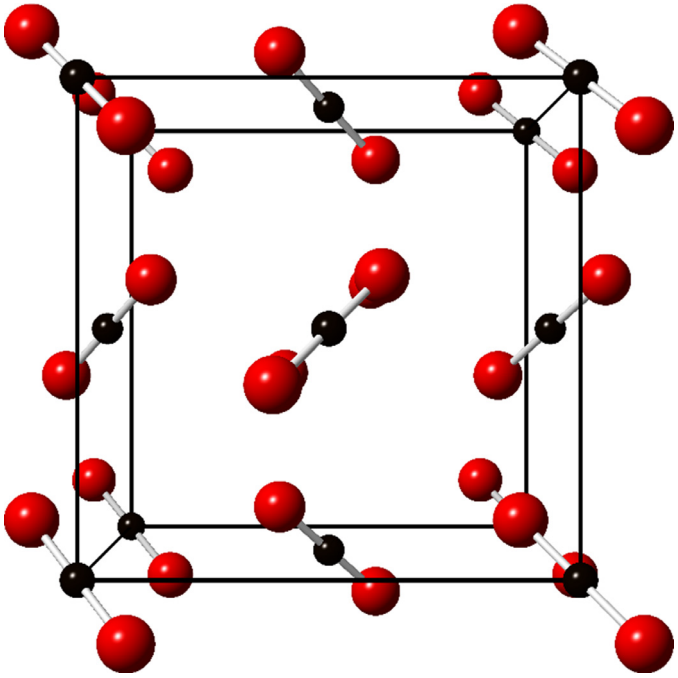

Fig. 1. The crystal structure of the unit cell of cubic CO_2-I. Carbon and oxygen atoms are indicated by the black and red spheres respectively. The whole crystal lattice can be built up by repetition of the unit cell in three dimensions. (For interpretation of the references to colour in this figure legend, the reader is referred to the web version of this article.)

form mostly during pre- and post-aphelion when the mesosphere is coldest, at temperatures often below 100 K. These extreme low temperatures are thought to be reached via gravity wave propagation, a process that is strongest at tropical latitudes (Creasey et al., 2006). These gravity waves cause cold pockets well below the CO_2 ice frost point temperature, within which heterogeneous nucleation of CO_2 ice is thought to trigger subsequent cloud formation (Gonzalez-Galindo et al., 2011; Listowski et al., 2014; Spiga et al., 2012). More optically thick CO_2 ice clouds (compared to the mesosphere) have been observed by the Mars Climate Sounder (MCS) at lower altitudes ($\leq$25 km) and higher temperatures (the frost point temperature is approximately 145 K at a surface pressure of 6 mbar) in the Martian polar winter troposphere (Hayne et al., 2012). The persistent presence of these CO_2 ice clouds below 20 km is apparent, and is thought to lead to the occurrence of CO_2 ice snowfall (Kuroda et al., 2013). This snowfall is likely to contribute in part to the formation of the CO_2 ice caps (Hayne et al., 2014).

The structure and thermodynamic properties of CO_2 ice are important for building a detailed understanding of the formation of these cloud types on Mars and therefore to help understand the Martian climate (and planet habitability) as a whole. This understanding is also pertinent for low temperature CO_2 ice formation throughout the interstellar medium and other planetary bodies, including exoplanets.

Parameters related to CO_2 crystal structure such as CO_2 ice density vary in the literature at low temperatures relevant to mesospheric CO_2 clouds. CO_2 ice has previously been described with a cubic structure with crystal symmetry of space group *Pa*-3 (No. 205) (de Smedt and Keesom, 1924). A single lattice parameter, a, is needed to describe the unit cell since $a = b = c$ and $\alpha = \beta = \gamma = 90°$ Consequently, the volume of the unit cell is calculated as a^3. The cubic symmetry of the unit cell can be seen in Fig. 1. The single lattice parameter of this ice (assigned as CO_2-I) has been previously determined with limited temperature resolution at low temperatures ($<$115 K) and under unknown deposition pressure conditions (Keesom and Kohler, 1934a, 1934b; Maass and Barnes, 1926). A temperature-independent CO_2 density value of 1.6 g cm^{-3} is often used in nucleation and modelling studies (Listowski et al., 2014, 2013; Maattanen et al., 2005, 2007; Wood, 1999). In fact, it is known that the density of CO_2-I ice is temperature dependent, but is poorly constrained through the Martian mesospheric temperature range. The commonly used CO_2 ice density value of 1.6 g cm^{-3} is applicable to 168 K, a temperature higher than is mesospherically relevant for CO_2 cloud formation, and is based originally on density values determined by Maass and Barnes (1926). This is significantly lower than density values determined for CO_2 ice at 83 K of 1.68 g cm^{-3} in a study by Keesom and Kohler (1934b) (later corrected by Curzon (1972)). Inaccuracies in the density value used for CO_2 ice may affect parameters such as ice nucleation, particle growth and sedimentation rates in experimental studies and models of CO_2 clouds. The temperature dependence of the CO_2 ice density may also be of importance for understanding past Martian climate, in which CO_2 clouds in an early denser atmosphere could have warmed the Martian surface sufficiently to allow for liquid water (Forget and Pierrehumbert, 1997; Forget et al., 2013; Mischna et al., 2000; Wordsworth et al., 2013).

The phase diagrams of some compounds, such as water ice, display complexity with the presence of multiple metastable and stable phases at low temperatures and pressures (Hobbs, 1974; Petrenko and Whitworth, 1999; Salzmann et al., 2011). For example, water ice is known to crystallise in a metastable stacking disordered form, ice I_{sd}, rather than the stable hexagonal form, at temperatures relevant for the Martian atmosphere (Malkin et al., 2015; Murray et al., 2015a). Stacking disordered ice is made up of cubic and hexagonal sequences in the crystal structure which are randomly arranged. This ice has a trigonal space group and is expected to form crystals with three-fold symmetry, in contrast to cubic ice which would be expected to form crystals with four-fold symmetry or hexagonal ice which forms crystals with six-fold symmetry (Murray et al., 2015b). Determination of low temperature phases of CO_2 ice or confirmation of an existing phase of relevance to ice formation in the Martian atmosphere is therefore worth investigating. To the best of the authors' knowledge, the CO_2 ice structure has never been previously determined experimentally under deposition (vapour to crystal, sometimes referred to as condensation) growth conditions analogous to the temperature and pressure conditions of clouds in the mesosphere of Mars.

In this study we performed laboratory experiments in which CO_2 vapour was deposited under Martian upper atmospheric temperatures (80–130 K) and pressures (0.01-1 mbar). Using X-ray diffraction (XRD) techniques and refinement methods we then determined the relevant crystal structure, lattice parameters, thermal expansion, density and probable crystal shape of CO_2 ice.

2. Methodology

In order to determine the CO_2 ice crystal structure under conditions relevant to the mesosphere of Mars, we examined ice growth on a temperature-controlled stage enclosed within an environmental chamber. This stage is probed using the powder X-ray diffraction (XRD) technique. In these experiments, CO_2 gas was either vapour deposited onto a flat substrate, or CO_2 in the form of powdered dry ice was placed in a sample holder and inserted into the chamber. We have previously used XRD to study vapour deposited water ice (Murray et al., 2015a; Shilling et al., 2006).

The X-Ray diffractometer (Bruker D8 Advance) was configured in a standard reflectance geometry and equipped with a Cu Kα X-ray source ($\lambda = 1.540598$ Å). Diffracted X-rays from a sample mounted on an Anton Paar TTK 450 temperature controlled stage were detected by a VÅNTEC detector (shown in Fig. 2). The use of Kapton-film windows sealed with O-rings allowed for the trans-

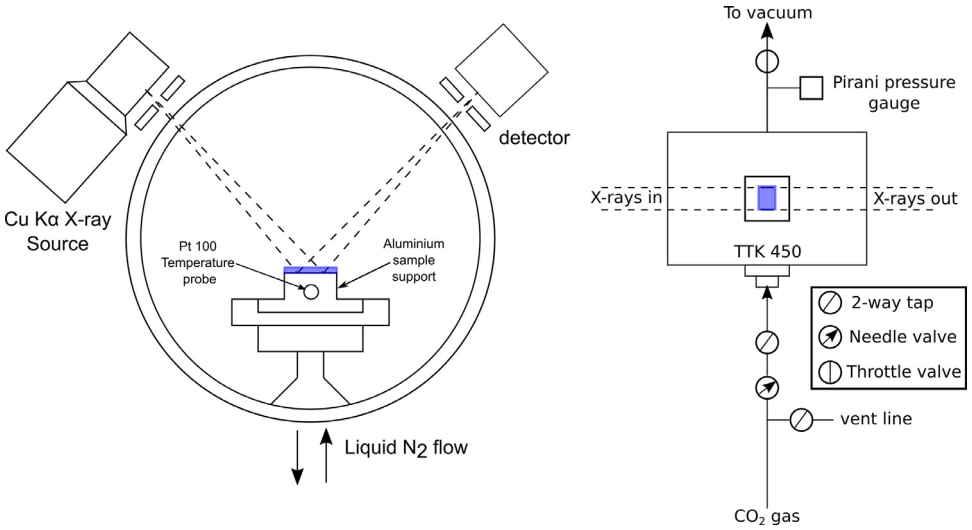

Fig. 2. Schematic diagrams of the front view of the TTK 450 temperature controlled stage (left) and top down view of the experimental system (right). The position of the CO_2 ice sample is indicated by the blue rectangle (not drawn to scale). (For interpretation of the references to colour in this figure legend, the reader is referred to the web version of this article.)

mission of X-rays in and out of the environmental chamber. The air-tight chamber was pumped by using a Pfeiffer Duo 2.5A vacuum pump allowing a pressure range of 1×10^{-3}–1×10^{3} mbar. This stage was cooled with liquid nitrogen pumped using a Thomas VTE 6 vacuum pump and the temperature was controlled using a Eurotherm PID controller and resistive heaters. The sample holder/support could be cooled to a stable sample temperature from ambient to 80 ± 0.2 K under pressures of < 2 mbar. The sample support was constructed from aluminium, covered with a borosilicate glass slide (160 µm thickness), and adhered to the aluminium support using a thin layer of vacuum grease. Temperature was measured using a Pt-100 probe directly inserted into the sample support. Heat conducting grease was used to maximise thermal contact between the probe and the sample support, as well as between the sample support and the cold stage, thus minimising temperature measurement error and maximising cooling efficiency.

In a typical vapour-deposition experiment the environmental chamber was first pumped to a pressure of $< 1 \times 10^{-2}$ mbar to ensure minimal water vapour contamination during cooling. The sample was then cooled from room temperature to 80 K at a rate of 20 K min^{-1}, at which temperature a diffraction pattern was recorded (2θ = 20-50°) to ensure no contamination in the form of water ice frosting had occurred on the glass slide. For CO_2 vapour deposition, a flow of pure CO_2 gas (Air Products CO_2 purity 4.5) was administered directly into the chamber via a needle valve. The environmental chamber was kept at low pressures during deposition (typically 0.01-1 mbar) using the vacuum pump and throttle valve. Low-resolution rapid XRD patterns were taken during deposition until significant signal was observed. The system was then sealed to maintain the pressure and high-resolution patterns with increments of $2\theta = 0.0426°$ were obtained at $2\theta = 20°$-50°. Experimental diffraction patterns were corrected against a silicon standard, accounting for peak shifting due to sample height.

For experiments looking at the structure of dry ice, an indented aluminium sample holder without a borosilicate glass slide was used. Dry ice was ground using a pestle and mortar and packed into the sample holder under liquid nitrogen, and dry argon gas was used to minimise water ice contamination. Grinding minimised the preferred orientation in the crystals. The environmental chamber was cooled to 80 K at vacuum in the absence of a sample holder and was flushed with dry N_2 before transferring the sample holder containing the dry ice into the chamber and promptly sealing it. XRD patterns were then taken across the scan range $2\theta = 20°$-50°.

3. Results and discussion

3.1. Crystal structure of CO_2 ice deposited from vapour

Fig. 3 shows diffraction patterns of typical vapour-deposited CO_2 ice at 80 K and 110 K, ground dry ice and a predicted pattern using known lattice parameters of CO_2-I with space group *Pa*-3 (taken from de Smedt and Keesom (1924)). Experiments were carried out at pressures as low as 0.01 mbar, corresponding to a Martian atmospheric pressure where CO_2 clouds have been observed at altitudes of approximately 65 km (Kleinbohl et al., 2009). The vapour-deposited ice at 80 K displays distinct Bragg peaks associated with a crystalline structure, consistent with previous studies suggesting that amorphous CO_2 only forms at temperatures below 50 K (Souda, 2006). The Bragg peaks in the vapour-deposited and dry ice samples are at comparable 2θ angles to the Bragg peaks in the predicted pattern. However, the 200 peak at 33° is absent in the vapour-deposited material at 80 K and the relative peak intensities vary between the measured (80 K and 110 K) and calculated pattern for an ideal powder.

In order to test if the diffraction pattern for the vapour-deposited ice is consistent with the CO_2-I phase it was necessary to use the Rietveld refinement method (Rietveld, 1969). Initially, the whole powder pattern decomposition was performed following the Pawley (1981) method (using the software package TOPAS 4.2) in order to confirm the fit to the CO_2-I literature crystal structure and determine the lattice parameters. The fit to the diffraction pattern in Fig. 3 shows that the ice generated via vapour deposition has a structure consistent with standard CO_2-I but with preferred orientation. Preferred orientation in powder diffraction patterns arises whenever there is a non-random orientation of crystallites in a sample. In order to obtain a perfect powder pattern, crystallites must be both numerous and randomly orientated. This produces diffraction rings and is amenable to standard powder XRD techniques where the detector only measures across a segment of the diffraction ring. In contrast, if a population of crystals all had identical crystallographic orientation, as might happen in epitaxial growth on a surface, then rather than obtaining diffraction rings, all the diffracted X-rays would be concentrated into spots with

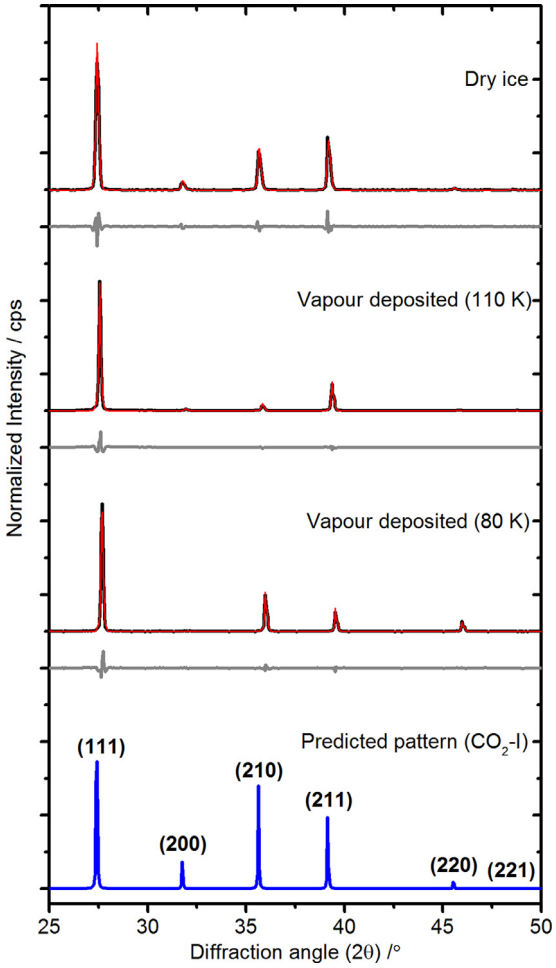

Fig. 3. Background corrected and vertically offset experimental XRD patterns of a typical vapour-deposited CO_2 ice at 80 K and 110 K, ground dry ice and a calculated XRD pattern based on current crystal structure for CO_2-I (de Smedt and Keesom, 1924). Profiles are normalised to the intensity of the 111 peak ($2\theta = \sim 27.5°$). The TOPAS refinement of the vapour-deposited and dry ice CO_2 patterns (black lines) for CO_2-I using the Pawley (1981) method is indicated by the red lines. The grey line shows the residuals of the fits. (For interpretation of the references to colour in this figure legend, the reader is referred to the web version of this article.)

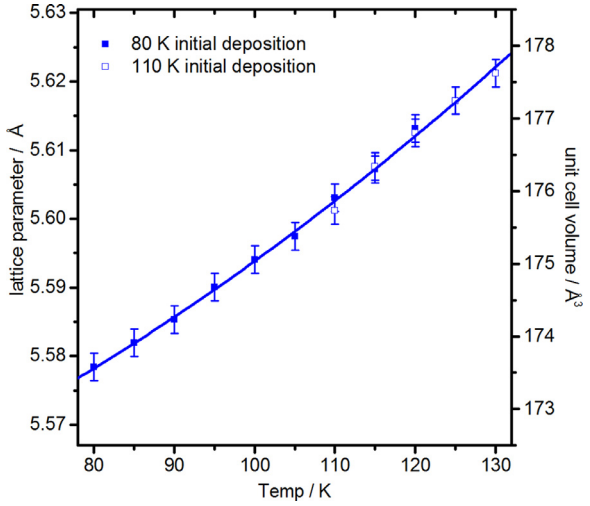

Fig. 4. CO_2-I lattice parameters and unit cell volumes for deposition at 80 K and 110 K. The blue line indicates a polynomial fit to the dataset.

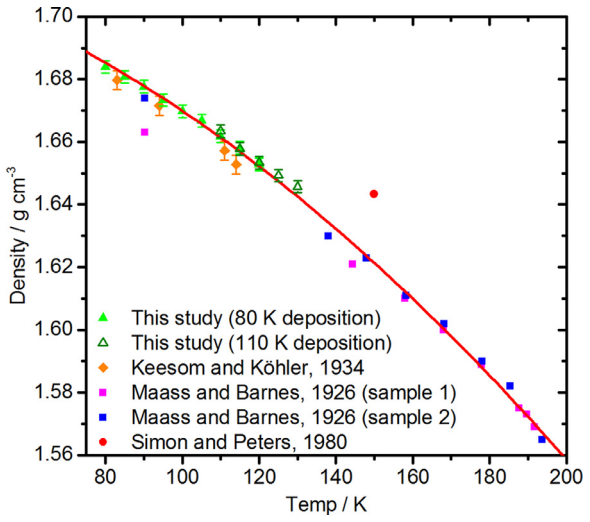

Fig. 5. CO_2 density values obtained from the lattice constants determined in this study as well as comparisons with literature values (Keesom and Kohler, 1934b; Maass and Barnes, 1926; Simon and Peters, 1980). The 2nd order polynomial fit is represented by the red line.

each spot corresponding to a specific crystallographic plane. In the case of this situation, the typical powder XRD instrument would not produce a meaningful diffraction pattern. Very commonly an intermediate situation exists where the crystallites are partially ordered, which results in Bragg peaks which can either be more or less intense than those in the ideal powder pattern and sometimes be missing all together. The analysis presented in Fig. 3 shows that patterns of the CO_2 ice we grew from the vapour phase and the powdered dry ice sample are consistent with the standard CO_2-I phase with varying degrees of preferred orientation.

In addition to using the Pawley (1981) refinement method the XRD patterns of vapour-deposited CO_2-I were also refined using the Le Bail et al. (1988) method. Although both are least-squares refinements, the method developed by Le Bail et al. (1988) treats the diffraction patterns without the need for peak intensities (while other crystallographic parameters are known), which in this case are affected by preferred orientation. The crystallographic properties calculated by both of these refinement methods agreed within error.

3.2. Temperature dependence of CO_2 ice structure and density

The temperature dependence of CO_2-I deposited from the vapour at 80 K (80-120 K) and 110 K (110–130 K) was determined and are summarised in Figs. 4 and 5 (parameters are also tabulated in the supplementary information). Deposited CO_2 ice layers were warmed at 1 K min^{-1} with diffraction patterns ($2\theta = 20° - 50°$, 2θ increment = 0.0426°) taken at 5 K intervals. It should be noted that the experiments in this study require a thin CO_2 film in good thermal contact, limiting the study to temperatures of ≤ 130 K because the ice film was lost to sublimation at higher temperatures. From subsequent refinement of these diffraction patterns, the temperature dependence of the lattice parameter and unit cell volume was determined for CO_2-I, shown in Fig. 4. The length of the lattice parameter (and therefore unit cell volume) increases with temperature due to thermal expansion of the crystal lattice.

The CO_2 ice densities were determined from changes in the unit cell volume with temperature. The results from this study and other literature values are shown in Fig. 5. We report a larger density (1.684 ± 0.002 g cm^{-3} at 80 K) when compared to the cor-

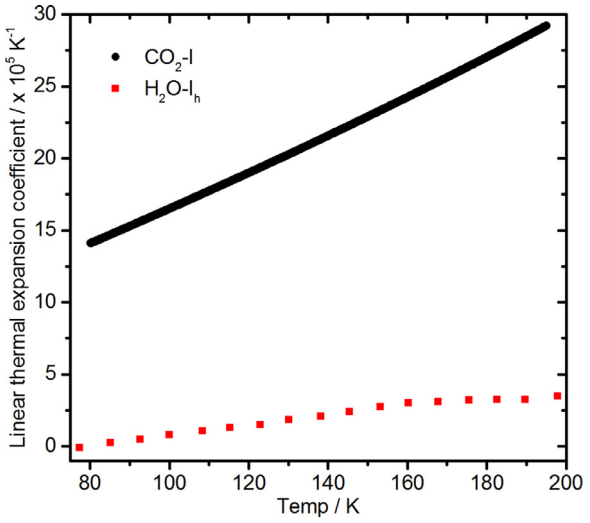

Fig. 6. Linear thermal expansion coefficients (x10^5) calculated for CO_2-I from the temperature-dependent density reported in this study and for H_2O-I_h using data reproduced from Röttger et al. (1994).

rected CO_2 density values of Keesom and Kohler (1934b) (where the lattice parameter values were converted from kX to Å (where 1 kX = 1.002 Å (Bragg, 1947) by Curzon (1972)). While one density value at 90 K from Maass and Barnes (1926) is in good agreement with the present study, the variability in the values determined when repeated (1.663-1.674 g cm^{-3} at 90 K) compared to the higher temperature densities (≥ 138 K) suggests errors in their method when applied to these low temperatures. It should be noted that in our density determination the temperature repeats from different experiments agree within error. The higher temperature values from Maass and Barnes (1926) follow a similar dependence to the lower temperature values determined in this study. A lattice parameter for CO_2 ice at 150 K based on a single crystal measurement by Simon and Peters (1980), when converted to a density, is in significant disagreement with our results and other literature density values (we note that no temperature uncertainties are given by Simon and Peters (1980)).

The density can be seen to decrease with increasing temperature which is consistent with the thermal expansion of CO_2 ice. A second-order polynomial fit through our data (80–130 K) and the Maass and Barnes (1926) data at temperatures ≥ 138 K yields the following equation of state for the CO_2 ice density at 1×10^{-2} mbar:

$$CO_2 \text{ density } (80 - 195 \text{ K}) = 1.72391 - 2.53 \times 10^{-4}\ T - 2.87 \times 10^{-6}\ T^2 \quad (1)$$

Using the temperature-dependent polynomial fit to the CO_2 density (Eq. (1)), linear thermal expansion coefficients were calculated from the volume expansivity for CO_2-I across 80–195 K and are shown in Fig. 6. The volume expansivity coefficient (β) is given by:

$$\beta = (1/V)(dV/dT) \quad (2)$$

where the linear expansivity coefficient (α) is then $(1/3)\beta$. The thermal expansion of CO_2 is compared to hexagonal H_2O ice (H_2O-I_h) over the same temperature range (Röttger et al., 1994). The thermal expansion of CO_2-I shows a positive gradient. Remarkably, it doubles over the temperature range (80 – 195 K) and is much larger compared to water ice. This rapid expansion for CO_2-I highlights the need for accurate temperature-dependent parameters.

3.3. Implications for Martian mesospheric CO_2 ice clouds

In this section the effect of crystal structure and density on the microphysics of mesospheric CO_2 clouds on Mars is explored. Initially, we determine the impact of using the temperature-dependent density data from this study compared to the previously used values of 1.5 g cm^{-3} and 1.6 g cm^{-3} taken from Luna et al. (2009) and Wood (1999), respectively (Listowski et al., 2014; Listowski et al., 2013; Maattanen et al., 2005; Nachbar et al., 2016). Certain CO_2 ice particle variables are linearly dependent on CO_2 ice density. This is illustrated, for example, by the Stokes sedimentation velocity (v_{sed}) as shown by Brasseur and Solomon (2006):

$$v_{sed} = \frac{2\rho g r^2 C_c}{9\eta} \quad (3)$$

where g is the gravitational constant for Mars, r the ice particle radius, η the viscosity of CO_2 gas and ρ the density of the CO_2 ice. C_c is the Cunningham slip factor, which corrects for the low atmospheric densities on Mars and therefore the transition to the free molecular regime. C_c taken from Listowski et al. (2014) is determined as $1 + Kn[1.246 + 0.42\ exp(-0.87/Kn)]$, where Kn is the Knudsen number, defined as the ratio of the mean free path over r. Using Eq. (3), the sedimentation velocities of particles with a range of CO_2 ice densities (where 1.684 g cm^{-3} is taken from the present study) were calculated as a function of particle radius. An extreme atmospheric temperature profile was used, consistent with the negative temperature perturbation that would be caused by a large amplitude gravity wave at ~80 km altitude (2×10^{-4} mbar and 80 K) (Kleinbohl et al., 2009; Listowski et al., 2014). Higher sedimentation velocities result from the higher density value found in this study, with the linear dependence of density on sedimentation causing a 5% increase in sedimentation velocity (1.6 g cm^{-3} compared to 1.684 g cm^{-3}). For example, under these conditions a spherical 500 nm radius ice particle falls an extra 1.6 km h^{-1} when the CO_2 ice density is increased from 1.6 to 1.684 g cm^{-3}. Extrapolating this to a population of CO_2 ice particles within a mesospheric cloud inside a cold pocket, unperturbed sedimentation would lead to a more rapid decrease in altitude of a detached CO_2 ice layer. This would result in shorter cloud lifetimes as the crystals fall into a warmer region below the cold pocket, causing rapid evaporation of the CO_2 ice particles (Listowski et al., 2014). In the case of tropospheric CO_2 clouds (10–100 μm particle radii) forming at temperatures ≤ 145 K, a density value higher than the current literature (1.6 g cm^{-3}) would also be required. Compared to current predictions, this would increase the precipitation rates of CO_2 ice particles from the cloud and hence affect the accumulation rate of CO_2 ice at the polar caps (Hayne et al., 2014).

Certain CO_2 ice parameters related to mesospheric Martian cloud microphysics have a greater complexity in terms of the effect of changing density values when compared to the linear effect on sedimentation. An example is the mechanism through which cloud ice particles are formed. Homogeneous nucleation of CO_2 is predicted to require very high supersaturation conditions and is thought to be an unlikely pathway to cloud formation in the Martian atmosphere (Maattanen et al., 2010, 2005). Heterogeneous ice nucleation via deposition of CO_2, in which the energy barrier to nucleation is reduced by the presence of an ice nucleating particle (INP), is thought to be the likely nucleation pathway (Nachbar et al., 2016). Heterogeneous nucleation is therefore applied here and is described in terms of classical heterogeneous nucleation theory induced by surface diffusion. CO_2 molecules are assumed to stick and subsequently diffuse to form clusters in INP; this may result in a critical cluster leading to stable nucleation of CO_2 ice on the particle. Described briefly here, the theory has been

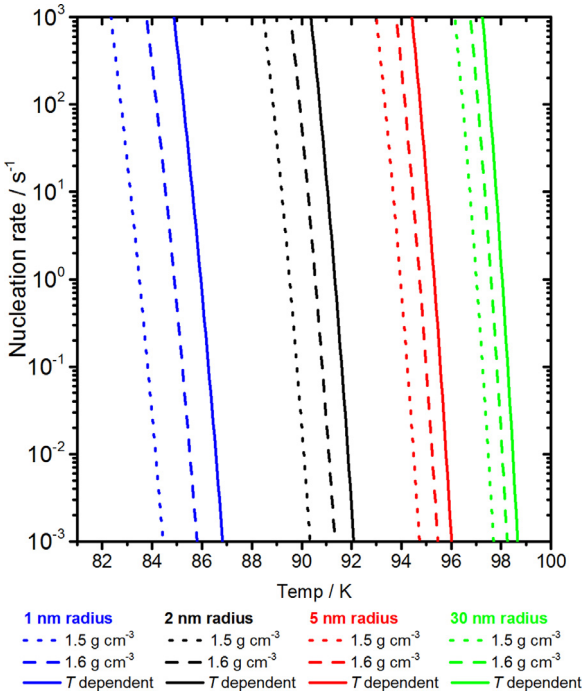

Fig. 7. Heterogeneous ice nucleation rates at variable CO_2 ice density (where "*T* dependent" indicates the temperature dependent-density fit produced in this study) for INP of selected radii between 1 and 30 nm. CO_2 concentrations were fixed at 10^{20} m^{-3}. (For interpretation of the references to colour in this figure legend, the reader is referred to the web version of this article.)

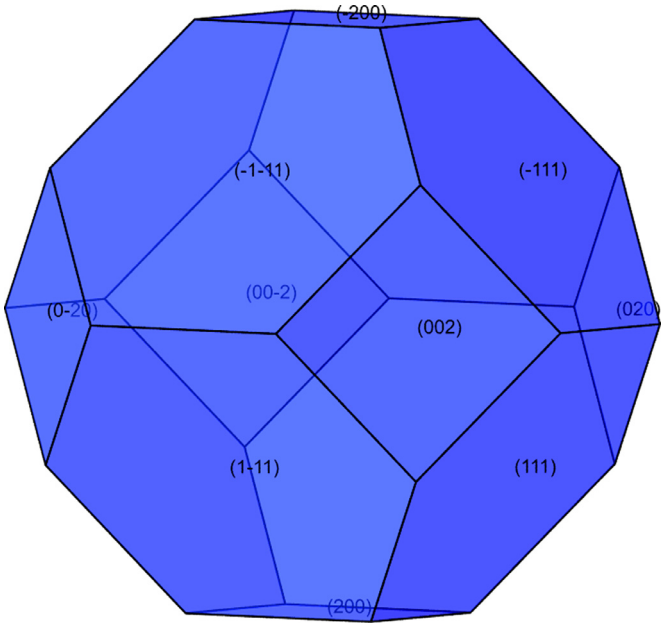

Fig. 8. Truncated octahedral crystal structure predicted for CO_2-I from BDFH analysis; the different crystallographic planes of the crystal are indicated in the brackets. This analysis indicates that some combination of the two families of faces, {111} and {200}, will be expressed on crystals of CO_2 ice. The potential range of crystal shapes which might be expressed is shown in Fig. 9.

previously applied to the study of CO_2 ice clouds (Listowski et al., 2014; Maattanen et al., 2005, 2007; Nachbar et al., 2016).

The rate of heterogeneous ice nucleation (J_{het}) for a spherical INP is given by:

$$J_{het} = A_N Z_{het} \beta_{het} c_{1,s} \exp\left(\frac{-\Delta F_{het}}{kT}\right) \quad (4)$$

where A_N is the surface area of the INP; Z_{het} is the heterogeneous Zeldovich factor which corrects for the dissociation of super-critical clusters; β_{het} accounts for the flux of CO_2 molecules on the INP *via* diffusion to form the critical cluster; $c_{1,s}$ is the concentration of monomers on the INP surface; and ΔF_{het} is the free energy of forming the critical cluster on the surface of the INP determined from the Gibbs–Thomson equation. ΔF_{het} is calculated in relation to the homogeneous form (ΔF_{hom}) with a reduction in the energy barrier by a factor $f(m,x)$ as described in Fletcher (1958), where x is the ratio of the size of the INP to the critical cluster and m is the contact parameter equal to cosθ, which relates to the contact angle between the INP and the nucleating phase. This complete ΔF_{het} description is given by:

$$\Delta F_{het} = f(m,x)\frac{16\pi v^2 \sigma^3}{3(kT\ \ln S)^2} \quad (5)$$

where v is the molecular volume in the condensed phase (m_m/ρ, where m_m is the mass of the molecule); σ the surface tension (0.08 J m^{-2} taken from Wood (1999)); and S the saturation ratio. Values for m (0.78) and ΔF_{des} (3.07×10^{-20} J molecule^{-1}, the desorption energy of CO_2 used to calculate $c_{1,s}$) are experimental values derived from a study of CO_2 nucleation on nanoparticles (Nachbar et al., 2016).

Application of this nucleation theory (Eqs. (4) and (5)) to heterogeneous nucleation rates of CO_2 on small INP analogous to meteoric material at high altitudes (1–30 nm radius particles) are shown in Fig. 7. Changes in CO_2 density alter the calculated values of the critical cluster, the number of molecules in the critical cluster and ΔF_{het}, which then impacts on the overall determined nucleation rates. The effect of shifting density is highlighted by the steep temperature dependence of the nucleation rates. Using the new temperature-dependent fit determined in this study (Eq. (1)) instead of the fixed value of 1.6 g cm^{-3} causes an approximately three-orders of magnitude increase in nucleation rate (at 85 K for a 1 nm radius INP). The impact of this density change reduces with increasing particle size, with nucleation rates on 30 nm radii INP increasing by 1–2 orders of magnitude. This increased nucleation rate using the new temperature dependent density values reduces the extent of negative temperature perturbations that would be required to initiate CO_2 cloud formation.

Finally, we also use the crystal structure of CO_2-I to predict possible crystal shapes of Martian CO_2 ice crystals. A range of crystal shapes have been suggested for the Martian atmosphere based on the crystal structure of CO_2-I ice. Theoretical predictions for the shape of CO_2 crystals on Mars include octahedrons, cubic and truncated octahedrons (Wood, 1999). Experimentally, CO_2 crystals grown on substrates were found to be dominantly octahedral (Foster et al., 1998).

We use the Bravais–Friedel–Donnay–Harker (BFDH) approach to predict the crystal shape (habit, or morphology) of CO_2 ice crystals from the crystallographic symmetry and lattice parameters. The BFDH approach assumes that the linear growth rate of a crystal face is inversely proportional to the corresponding interplanar distance (Donnay and Harker, 1937). Consequently, faces with the smallest Miller indices, which have the largest interplanar distances, will grow the slowest. Faces with higher Miller indices will expose more dangling bonds and be less stable, grow faster and therefore 'grow out' quickly leaving crystals only expressing the lower energy, lower Miller index faces. The BFDH approach predicts that the {200} and the {111} families of faces will be expressed in crystals of CO_2 ice and this results in a truncated octahedron shape (see Fig. 8). In real crystals, significant deviations from the BFDH model can occur. These are due to the exact details of the chemical interactions between molecules which can

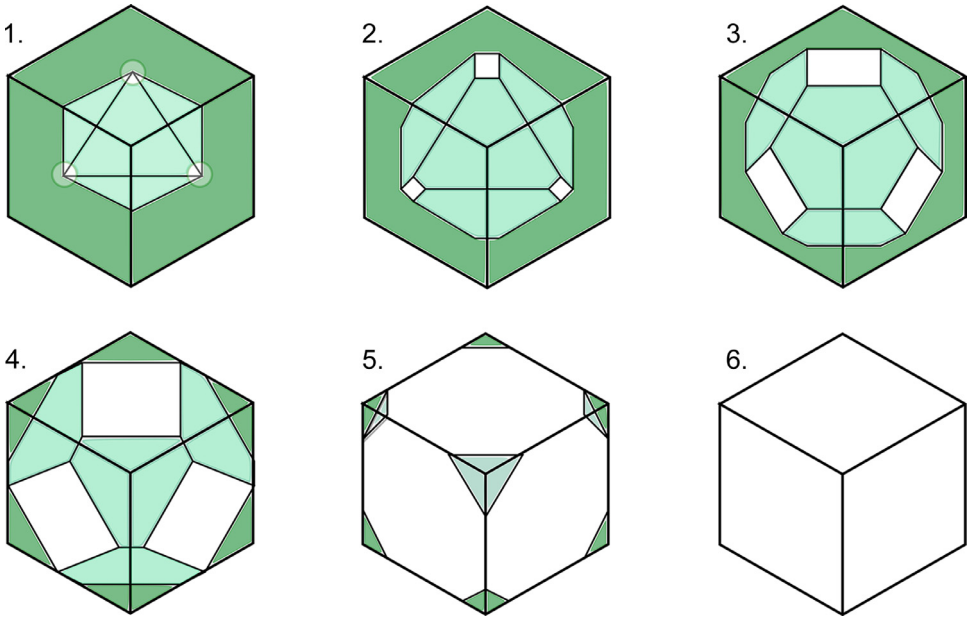

Fig. 9. Illustration of how an octahedral crystal shape is related to a cube in which all shapes shown have the same point group (O_h) related to the space group of CO_2-I). A cube results if the growth rate of the {111} family of faces grows more rapidly than the {200} family of faces, whereas an octahedron results if the opposite is true. If the growth rates of the two groups of faces are comparable, a cubo-octahedral crystal forms. In the literature octahedra of cubic ice are sometimes referred to as bi-pyramidal. Octahedra is a more specific term since the {111} faces of octahedra are equilateral triangles, whereas bi-pyramidal shapes can have triangular faces that are not equilateral.

be highly anisotropic and consequently lead to deviations of the growth rates from the simple inverse relationship with interplanar distance used in the BFDH approach. In the case of CO_2-I this means that crystal shapes can deviate from the idealised cubo-octahedral shape in Fig. 8.

Ice crystals in the Earth's atmosphere can take on a wide range of forms, from compact hexagonal plates and columns to the huge array of dendritic snowflakes; the crystal shape depending on temperature and supersaturation. Crystal shape is important because it influences crystal fall speeds, growth rates and their optical properties. In fact, Foster et al. (1998) demonstrated that extinction, absorption and scattering efficiencies in the IR are sensitive to crystal shape. It is thought that CO_2 ice crystals in the Martian atmosphere are unlikely to form dendrites since dendritic structures form when crystal growth becomes diffusion limited. For CO_2 ice crystals in the Martian atmosphere which is dominantly composed of CO_2, diffusion limitation is unlikely (Wood, 1999). Hence, Martian CO_2 ice crystals are likely to be compact crystals and the BFDH model demonstrates that these crystals may have two families of faces exposed – the six-sided {111} family of faces and the four-sided {200} family. But, as with compact water ice crystals (Murray et al., 2015b), CO_2 ice may still exhibit a range of crystal shapes if the relative growth rates of the two groups of faces vary. The possible crystal shapes, all with the same O_h point group (derived from the space group of CO_2-I), are shown in Fig. 9. If the {111} family of faces grows faster than the {200} family then a crystal in the shape of a cube would be expected, whereas if the opposite is the case then an octahedron crystal would form. It is also possible that the growth rates of the two sets of equivalent faces are competitive in which case a cubo-octahedron would form. Close inspection of the images of CO_2 ice crystals in Foster et al. (1998) reveal that while some crystals are clearly octahedral, others are truncated with square faces which are consistent with cubo-octahedra. In summary, in the Martian atmosphere we might expect CO_2 crystals with a range of morphologies, from cubic to octahedral, and the exact crystal shapes which exist there may depend on temperature and supersaturation of the atmosphere from which they grow as well as any effect of latent heat release on the temperature of the growing crystal.

Deposition of CO_2 ice directly onto the Martian surface occurs in the polar regions and is responsible for seasonal pressure fluctuations. Our results indicate that this ice is also the standard CO_2-I phase. Laboratory simulations of ice deposits suggest that at low pressures and under Martian temperatures (~130–145 K) the ice forms a translucent slab, whereas at lower temperatures it forms 'triangular' crystals (Portyankina et al., 2016) (Note that those authors use the term 'crysalline structures' to mean the morphology of the ice they generate, whereas we use the term 'crystal structure' to define the regular arrangement of atoms in a crystal). When CO_2 ice crystals fall from the atmosphere and accumulate at the surface they will most likely anneal to minimise gas-solid interfacial area which minimises surface free energy. Portyankina et al. (2016) note that cracks in CO_2 ice anneal (disappear) in only minutes which indicates that annealing processes could be quite rapid. Hence, CO_2 ice particles will likely lose their initial shape once on the ground, much like ice crystals in snow pack on Earth evolves with time.

4. Summary and conclusions

In this study the first XRD diffraction patterns of CO_2 ice, deposited under temperature and pressure conditions analogous to the Martian mesosphere are presented. A cubic crystal structure consistent with previous literature determinations of CO_2-I with *Pa*-3 space group has been found under all conditions studied. Analysis of the diffraction patterns gave a lattice parameter of 5.578 ± 0.002 Å, a unit cell volume of 173.554 ± 0.19 Å^3 and density of 1.684 ± 0.002 g cm^{-3} at 80 K. From the diffraction data, the density was determined from 80 to 130 K and combined with literature data to give a polynomial fit valid from 80 to 195 K (CO_2 density $= 1.72391 - 2.53 \times 10^{-4}\,T - 2.87 \times 10^{-6}\,T^2$). This equation of state was applied to sedimentation and ice nucleation rates relevant to CO_2 ice clouds in the mesosphere of Mars. We suggest that the new temperature-dependent equation of state is used in future modelling studies of CO_2 ice in the Martian atmosphere. Finally, the crystal morphology of solid CO_2 was predicted using the BFDH approach, suggesting that Martian CO_2 ice crystals could take the shape of a cube, an octahedron or a cubo-octahedron.

Acknowledgements

TPM thanks the Natural Environment Research Council (NERC) for a PhD studentship and thanks Mario Nachbar for discussions regarding CO_2 nucleation. BJM thanks that European Research Council for funding (ERC, 240449 ICE; 648661 MarineIce). CGS thanks the Royal Society for a University Research Fellowship (UF100144).

Supplementary materials

Supplementary material associated with this article can be found, in the online version, at doi:10.1016/j.icarus.2017.03.012.

References

Bragg, W.L., 1947. The conversion factor for kX units to ångström units. J. Sci. Instrum. 24, 27.
Brasseur, G.P., Solomon, S., 2006. Aeronomy of the Middle Atmosphere: Chemistry and Physics of the Stratosphere and Mesosphere. Springer Science & Business Media.
Byrne, S., Ingersoll, A.P., 2003. A sublimation model for martian south polar ice features. Science. 299, 1051–1053.
Chiar, J.E., 1997. The nature and evolution of interstellar ices. Origins Life Evol. Biosph. 27, 79–100.
Clancy, R.T., et al., 2007. Mars equatorial mesospheric clouds: global occurrence and physical properties from Mars global surveyor thermal emission spectrometer and Mars orbiter camera limb observations. J. Geophys. Res. Planets. 112.
Creasey, J.E., et al., 2006. Global and seasonal distribution of gravity wave activity in Mars' lower atmosphere derived from MGS radio occultation data. Geophys. Res. Lett. 33.
Curzon, A.E., 1972. A comment on the lattice parameter of solid carbon dioxide at -190 °C. Physica. 59, 733.
de Smedt, J., Keesom, W.H., 1924. The structure of solid nitrous oxide and carbon dioxide. In: Proceedings of the Koninklijke Akademie Van Wetenschappen Te Amsterdam, 27, pp. 839–846.
Donnay, J.D.H., Harker, D., 1937. A new law of crystal morphology extending the law of bravais. J. Mineralog. Soc. Am. 22, 446–467.
Fletcher, N.H., 1958. Size effect in heterogeneous nucleation. J. Chem. Phys. 29, 572–576.
Forget, F., Pierrehumbert, R.T., 1997. Warming early Mars with carbon dioxide clouds that scatter infrared radiation. Science. 278, 1273–1276.
Forget, F., et al., 2013. 3D modelling of the early martian climate under a denser CO_2 atmosphere: temperatures and CO_2 ice clouds. Icarus. 222, 81–99.
Foster, J.L., et al., 1998. Carbon dioxide crystals: An examination of their size, shape, and scattering properties at 37 GHz and comparisons with water ice (snow) measurements. J. Geophys. Res. Planets. 103, 25839–25850.
Gonzalez-Galindo, F., et al., 2011. The martian mesosphere as revealed by CO_2 cloud observations and general circulation modeling. Icarus. 216, 10–22.
Hayne, P.O., et al., 2014. The role of snowfall in forming the seasonal ice caps of Mars: models and constraints from the Mars climate sounder. Icarus. 231, 122–130.
Hayne, P.O., et al., 2012. Carbon dioxide snow clouds on Mars: South polar winter observations by the Mars climate sounder. J. Geophys. Res. Planets 117.
Herr, K.C., Pimentel, G.C., 1970. Evidence for solid carbon dioxide in upper atmosphere of Mars. Science. 167, 47–49.
Hobbs, P.V., 1974. Ice Physics. Clarendon Press, Oxford.
Johnson, R.E., 1996. Sputtering of ices in the outer solar system. Rev. Modern Phys. 68, 305–312.
Keesom, W.H., Kohler, J.W.L., 1934a. The lattice constant and expansion coefficient of solid carbon dioxide. Physica. 1, 655–658.
Keesom, W.H., Kohler, J.W.L., 1934b. New determination of the lattice constant of carbon dioxide. Physica. 1, 167–174.
Kleinbohl, A., et al., 2009. Mars Climate Sounder limb profile retrieval of atmospheric temperature, pressure, and dust and water ice opacity. J. Geophys. Res. Planets. 114.
Kuroda, T., et al., 2013. Carbon dioxide ice clouds, snowfalls, and baroclinic waves in the northern winter polar atmosphere of Mars. Geophys. Res. Lett. 40, 1484–1488.
Le Bail, A., et al., 1988. Ab-initio structure determination of $LiSbWO_6$ by X-ray powder diffraction. Mater. Res. Bullet. 23, 447–452.
Leighton, R.B., Murray, B.C., 1966. Behavior of carbon dioxide and other volatiles on Mars. Science. 153, 136–144.
Listowski, C., et al., 2014. Modeling the microphysics of CO_2 ice clouds within wave-induced cold pockets in the martian mesosphere. Icarus. 237, 239–261.
Listowski, C., et al., 2013. Near-pure vapor condensation in the Martian atmosphere: CO_2 ice crystal growth. J.Geophys. Res. Planets. 118, 2153–2171.
Luna, R., et al., 2009. Triple test under high vacuum conditions to control the reliability of thin ice film accretion and desorption for astrophysical applications. Vacuum. 83, 942–948.
Maass, O., Barnes, W.H., 1926. Some thermal constants of solid and liquid carbon dioxide. In: Proceedings of the Royal Society of London Series a-Containing Papers of a Mathematical and Physical Character, 111, pp. 224–244.
Maattanen, A., et al., 2010. Mapping the mesospheric CO_2 clouds on Mars: MEx/OMEGA and MEx/HRSC observations and challenges for atmospheric models. Icarus. 209, 452–469.
Maattanen, A., et al., 2005. Nucleation studies in the Martian atmosphere. J. Geophys. Res. Planets 110.
Maattanen, A., et al., 2007. Two-component heterogeneous nucleation kinetics and an application to Mars. J. Chem. Phys. 127.
Malkin, T.L., et al., 2015. Stacking disorder in ice I. Phys. Chem. Chem. Phys. 17, 60–76.
McConnochie, T.H., et al., 2010. THEMIS-VIS observations of clouds in the Martian mesosphere: altitudes, wind speeds, and decameter-scale morphology. Icarus. 210, 545–565.
McCord, T.B., et al., 1998. Non-water-ice constituents in the surface material of the icy Galilean satellites from the Galileo near-infrared mapping spectrometer investigation. J. Geophys. Res. Planets. 103, 8603–8626.
Mischna, M.A., et al., 2000. Influence of carbon dioxide clouds on early Martian climate. Icarus. 145, 546–554.
Montmessin, F., et al., 2006. Subvisible CO_2 ice clouds detected in the mesosphere of Mars. Icarus. 183, 403–410.
Montmessin, F., et al., 2007. Hyperspectral imaging of convective CO_2 ice clouds in the equatorial mesosphere of Mars. J. Geophys. Res. Planets. 112.
Murray, B.J., et al., 2015a. The crystal structure of ice under mesospheric conditions. J. Atmosph. Solar Terrestrial Phys. 127, 78–82.
Murray, B.J., et al., 2015b. Trigonal ice crystals in Earth's atmosphere. Bull. Am. Meteorol. Soc. 96, 1519–1531.
Nachbar, M., et al., 2016. Laboratory measurements of heterogeneous CO_2 ice nucleation on nanoparticles under conditions relevant to the Martian mesosphere. J. Geophys. Res. 121, 753–769.
Pawley, G.S., 1981. Unit-cell refinement from powder diffraction scans. J. Appl. Crystallogr. 14, 357–361.
Petrenko, V.F., Whitworth, R.W., 1999. Physics of Ice. Oxford University Press, Oxford; New York.
Portyankina, G., et al., 2016. laboratory investigations of physical state of CO2 ice on mars. Sixth Mars Polar Science Conference.
Rietveld, H.M., 1969. A profile refinement method for nuclear and magnetic structures. J. Appl. Crystallogr. 2, 65–71.
Röttger, K., et al., 1994. Lattice-constants and thermal-expansion of H2o and D2o Ice Ih between 10 and 265 K. Acta Crystallographica Sect. B Struct. Sci. 50, 644–648.
Salzmann, C.G., et al., 2011. The polymorphism of ice: five unresolved questions. Phys. Chem. Chem. Phys. 13, 18468–18480.
Sefton-Nash, E., et al., 2013. Climatology and first-order composition estimates of mesospheric clouds from Mars climate sounder limb spectra. Icarus. 222, 342–356.
Shilling, J.E., et al., 2006. Measurements of the vapor pressure of cubic ice and their implications for atmospheric ice clouds. Geophys. Res. Lett. 33.
Simon, A., Peters, K., 1980. Single-crystal refinement of the structure of carbon-dioxide. Acta Crystallographica Sect. B Struct. Sci. 36, 2750–2751.
Souda, R., 2006. Glass-liquid transition of carbon dioxide and its effect on water segregation. J. Phys. Chem. B. 110, 17884–17888.
Spiga, A., et al., 2012. Gravity waves, cold pockets and CO_2 clouds in the Martian mesosphere. Geophys. Res. Lett. 39.
Tillman, J.E., et al., 1993. The Martian annual atmospheric-pressure cycle - years without great dust storms. J. Geophys. Res. Planets. 98, 10963–10971.
Vincendon, M., et al., 2011. New near-IR observations of mesospheric CO_2 and H_2O clouds on Mars. J. Geophys. Res. Planets. 116.
Wood, S.E., 1999. Nucleation and Growth of Carbon Dioxide Ice Crystals in the Martian Atmosphere. University of California, Los Angeles.
Wordsworth, R., et al., 2013. Global modelling of the early Martian climate under a denser CO_2 atmosphere: water cycle and ice evolution. Icarus. 222, 1–19.